Available online at www.sciencedirect.com
ScienceDirect
Journal of Molecular Catalysis A: Chemical 268 (2007) 169–175
JOURNAL OF MOLECULAR CATALYSIS A: CHEMICAL
www.elsevier.com/locate/molcata

Activity and characterization of modified Cr_2O_3/ZrO_2 nano-composite catalysts for oxidative dehydrogenation of ethane to ethylene with CO_2

Shuang Deng [a,*], Huiquan Li [b], Songgeng Li [a], Yi Zhang [b]

[a] *Department of Chemical and Biomolecular Engineering, Ohio State University, 140 West 19th Avenue, Columbus, OH 43210, USA*
[b] *Institute of Process Engineering, Chinese Academy of Sciences, Beijing 100080, PR China*

Received 15 November 2006; received in revised form 17 December 2006; accepted 18 December 2006
Available online 23 December 2006

Abstract

Cr_2O_3/ZrO_2 nano-composite catalysts modified with Ni, Fe, Co, Mn oxides respectively were synthesized by coupling co-precipitation with azeotropic distillation method. The effect of modifiers on the catalytic activity in the dehydrogenation of ethane with CO_2 was investigated. The modifiers exhibited different effects on catalytic behavior. Fe, Co and Mn oxides markedly increased ethylene selectivity, but the Ni_5-Cr_{10}/Zr nano-composite catalyst mainly favored side reactions—the reforming and cracking reactions. The Fe_5-Cr_{10}/Zr nano-composite catalyst exhibited an excellent performance in this reaction, producing 50.05% ethylene yield at 53.72% ethane conversion at 650 °C. The modified Cr_2O_3/ZrO_2 nano-composite catalysts were characterized by BET, TEM, XRD, XPS, CO_2-TPD and NH_3-TPD techniques. The characterization indicated that weak acid sites are involved in ethane activation, and strong acid–base pairs promote the reforming and cracking reactions. The distribution of chromium species, oxygen species and base/acid property on the surface of catalyst cooperatively determined the catalytic activity in dehydrogenations of ethane to ethylene using CO_2 as an oxidant.

Keywords: Cr_2O_3/ZrO_2 nano-composite catalyst; Modifier; CO_2; Dehydrogenation; Ethane; Ethylene

1. Introduction

Carbon dioxide is one of the major greenhouse gases. The utilization of carbon dioxide has attracted an intensive attention in academia and industry. Recently several attempts have been made to utilize carbon dioxide as a mild oxidant for dehydrogenation of ethane to yield ethylene because of the growing requirement for alkenes [1–10]. This process provides several advantages, which had been demonstrated by many researchers [1,6,7], such as a lower reaction temperature and less catalyst deactivation due to coking. Furthermore, syn-gas can be obtained as a by-product of this process. Up to now, Fe-Mn/Si-2 [1], La_2O_3/γ-Al_2O_3 [2], Mo_2C/SiO_2 [4], Cr/H-ZSM-5 [5], K-Cr-Mn/SiO_2 [6], Cr/SiO_2 [7], Ga/TiO_2 [8], CeO_2-based [9] and metal oxides [10] catalysts have been used in the dehydrogenation of ethane with CO_2 as an oxidant. Among these catalysts, chromium-based catalysts have proven to be the most effective catalysts for this reaction [5–7]. In order to obtain better catalytic activity, some efforts had been focused on the supports of chromium-based catalysts using TS-1 [11] and MSU-*x* [12].

In the past decade, nano-particles (especially, oxides) attracted much attention in the field of heterogeneous catalysis due to their unique physical and chemical properties. Many efforts were devoted to prepare nano-particle catalysts and a number of interesting results were obtained for different catalytic reactions [13–15]. Compared to other Cr_2O_3-based nano-composite catalysts for the oxidative dehydrogenation of ethane to ethylene with CO_2, the Cr_2O_3/ZrO_2 nano-composite catalysts showed high catalytic activity with low selectivity to ethylene in our prior research [15]. The objective of this work is to attempt to improve the ethylene selectivity in the dehydrogenation of ethane with CO_2 on the Cr_2O_3/ZrO_2 nano-composite catalyst with the addition of Fe, Ni, Mn, and Co oxides. Chemical and structural properties of these catalysts were characterized and these results were used to establish a correlation with their catalytic activity.

* Corresponding author. Fax: +1 614 292 3769.
E-mail address: deng.55@OSU.edu (S. Deng).

1381-1169/$ – see front matter © 2007 Elsevier B.V. All rights reserved.
doi:10.1016/j.molcata.2006.12.033

2. Experimental

2.1. Catalyst preparation

The modified Cr_2O_3/ZrO_2 nano-composite catalysts were prepared by coupling co-precipitation with the azeotropic distillation method. Mixed solution of $CrCl_3$, $FeCl_3$, and $ZrOCl_2$ and diluted $NH_3{\cdot}H_2O$ solution were simultaneously added dropwise into a diluted $NH_3{\cdot}H_2O$ solution (pH ≈ 10) at 40 °C with stirring. The precipitates were filtered and washed with deionized water until no Cl^- was detected using a 0.1 M $AgNO_3$ solution, then *n*-butyl alcohol was added to remove residual water from the precipitates with azeotropic distillation. After vacuum-drying at 80 °C for 8 h and calcination at 600 °C in air for 2.5 h, the Fe_5-Cr_{10}/Zr nano-composite was prepared. The nano-particles of Fe_5-Cr_{10}/Zr were pressed, crushed and sieved into catalysts of 20–40 mesh. The Mn_5-Cr_{10}/Zr, Ni_5-Cr_{10}/Zr and Co_5-Cr_{10}/Zr nano-composite catalysts were prepared using a similar method.

2.2. Catalyst characterization

BET surface area, pore size and pore volumes of the samples were determined using N_2 adsorption method on an Autosorb-1 physisorb analyzer. X-ray diffraction (XRD) patterns of the catalysts were obtained on a Rigaku D/max-2400 X-ray diffractometer at 40 kV and 120 mA; using Ni filtered Kα radiation from a Cu target. The size of the nano-particles was determined using a HITACHI H-8100 TEM. XPS measurements were carried out on a PHI 5300/ESCA system (Perkin-Elmer) with Al Kα as a radiation source. Data were acquired at 25 mA under the vacuum of 2.9×10^{-7} Pa.

NH_3- and CO_2-TPD tests were performed using a Chembet-3000 chemisorb analyzer. The catalysts (0.1 g) were treated at 400 °C for 4 h in a helium flow of 30 ml/min. The pretreated samples were saturated with a NH_3 or CO_2 flow (15 ml/min) at room temperature for 1 h. The samples were flushed with Ar flowing at 20 ml/min for 30 min; then the temperature was increased to 1000 °C at a heating rate of 18 °C/min. Gases desorbed were monitored using a thermal conductivity detector (TCD). The amounts of basic/acidic sites on the surface of the catalyst were estimated by the desorption quantities of CO_2/NH_3, which was determined by the areas of the desorption profiles.

2.3. Catalytic tests

The catalytic tests were performed in a fixed-bed flow type quartz reactor packed with 200 mg of the catalyst and 1 g of quartz sand at atmospheric pressure. The reactant stream consisting of 20% ethane, 60% carbon dioxide and 20% Ar was introduced into the reactor at a flow rate of 15 ml/min. The reaction temperature ranged between 550 and 650 °C. The products were analyzed on line by a gas chromatograph (Shimadzu GC 14B) with a Porapak QS column and a 5 A molecular sieve column.

3. Results and discussion

3.1. Catalytic performance

CO, H_2, CH_4 and water were detected in addition to ethylene in the catalytic tests. Based on this result and other proposed reaction pathways [1,7], the overall reactions can be described as follows:

$$C_2H_6 \rightarrow C_2H_4 + H_2 \quad (1)$$

$$CO_2 + H_2 \rightarrow CO + H_2O \quad (2)$$

$$C_2H_6 + CO_2 \rightarrow C_2H_4 + CO + H_2O \quad (3)$$

$$C_2H_6 + 2CO_2 \rightarrow 4CO + 3H_2 \quad (4)$$

Table 1
Catalytic performance of various Cr_2O_3/ZrO_2 nano-composite catalysts

Catalysts	T (°C)	Conversion (%)		Selectivity (%)		Yield (%) C_2H_4
		C_2H_6	CO_2	C_2H_4	CH_4	
Cr_2O_3/ZrO_2	550	37.25	21.97	78.25	8.70	29.15
	600	63.43	32.50	55.34	12.1	35.10
	650	77.47	35.72	46.34	15.7	35.90
Fe_5-Cr_{10}/Zr	550	18.38	6.27	98.35	1.46	18.08
	600	31.24	10.05	95.41	4.53	29.81
	650	53.72	16.13	93.17	6.74	50.05
Ni_5-Cr_{10}/Zr	550	90.65	40.12	8.20	21.94	7.43
	600	95.11	50.35	3.76	15.83	3.58
	650	96.32	58.09	0	10.68	0
Mn_5-Cr_{10}/Zr	550	15.95	5.54	98.03	1.89	15.64
	600	26.39	9.59	94.10	4.65	24.83
	650	46.97	14.13	91.61	8.13	43.03
Co_5-Cr_{10}/Zr	550	19.89	2.08	95.40	3.72	18.98
	600	36.44	10.12	90.31	10.68	32.91
	650	61.42	23.78	79.53	16.21	48.85

Reaction conditions—CO_2:C_2H_6:Ar = 3:1:1; flow rate = 15 ml/min; 0.2 g catalysts; P = 0.1 MPa; GHSV = 4500 ml h^{-1} g^{-1}.

$$C_2H_6 + H_2 \rightarrow 2CH_4 \quad (5)$$

The ethylene was produced by the direct dehydrogenation of ethane (1) and the oxidative dehydrogenation of ethane with CO_2 (3), which could also be seen as the ethane dehydrogenation reaction (1) coupled with the reverse water-gas shift reaction (2). The reforming reaction (4) and hydrocracking of ethane (5) were side reactions. Table 1 presents the catalytic conversions and selectivity of oxidative dehydrogenations of ethane with CO_2 to ethylene over modified and unmodified Cr_2O_3/ZrO_2 nano-composite catalysts at various temperatures. Catalytic conversion increased and ethylene selectivity decreased with elevation of reaction temperature. The ethylene selectivity of the Fe_5-Cr_{10}/Zr, Mn_5-Cr_{10}/Zr and Co_5-Cr_{10}/Zr nano-composite catalysts was markedly higher than that of the Cr_2O_3/ZrO_2 nano-composite catalyst, while their ethane and CO_2 conversions were lower than that of the Cr_2O_3/ZrO_2 nano-composite catalyst. Inversely, the Ni_5-Cr_{10}/Zr nano-composite catalyst showed the highest ethane and CO_2 conversions, much higher than even the Cr_2O_3/ZrO_2 nano-composite catalyst, while it demonstrated the lowest selectivity to ethylene among the prepared catalysts. The high yield of CO and high selectivity to methane indicated that the Ni_5-Cr_{10}/Zr nano-composite catalyst favored the reforming reaction (4) and the cracking reaction (5). The Fe_5-Cr_{10}/Zr, Mn_5-Cr_{10}/Zr and Co_5-Cr_{10}/Zr nano-composite catalysts did not favor the reforming reaction, especially below 600 °C. Among the prepared catalysts, the Fe_5-Cr_{10}/Zr nano-composite catalyst exhibited not only high ethylene selectivity, but also relatively high ethane and CO_2 conversions. At 650 °C, the Fe_5-Cr_{10}/Zr nano-composite catalyst demonstrated 93.17% ethylene selectivity and 53.72% ethane conversion.

3.2. Textural and structural properties

BET surface area, average pore size and pore volumes of various Cr_2O_3/ZrO_2 nano-composites are given in Table 2. The pore volumes of modified Cr_2O_3/ZrO_2 nano-composites significantly increased, and were almost double value of the Cr_2O_3/ZrO_2 nano-composites. Compared with the variation of pore volume, the surface area of the Cr_2O_3/ZrO_2 nano-composite changed little with the addition of modifiers. The average pore sizes of the modified nano-composites were larger than that of the Cr_2O_3/ZrO_2 nano-composite.

The XRD patterns of modified Cr_2O_3/ZrO_2 nano-composites are presented in Fig. 1. Only tetragonal ZrO_2 can be observed in the Fe_5-Cr_{10}/Zr, Mn_5-Cr_{10}/Zr and Co_5-Cr_{10}/Zr nano-composites, which mean that the Fe, Mn and Co oxides did not change the crystal structure of the Cr_2O_3/ZrO_2 nano-composite

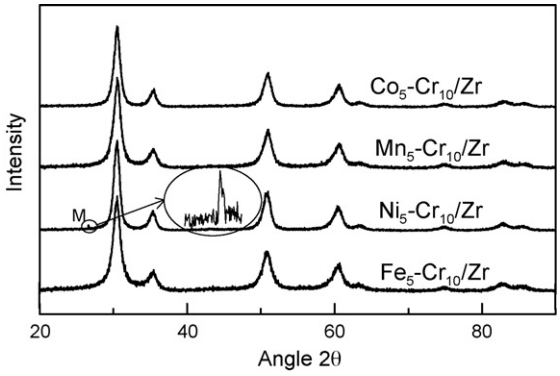

Fig. 1. XRD patterns of the modified Cr_2O_3/ZrO_2 nano-composite catalysts.

[15]. Monoclinic and tetragonal ZrO_2 coexisted in the Ni_5-Cr_{10}/Zr nano-composite, while tetragonal ZrO_2 was the major phase. This suggests that addition of Ni oxide induced the phase transformation of tetragonal ZrO_2 to monoclinic ZrO_2. According to Bachiller-Baeza and Jung [16,17], the monoclinic structure of ZrO_2 brings about stronger surface adsorption sites for CO_2 than the tetragonal structure. In this investigation, only the Ni_5-Cr_{10}/Zr nano-composite exhibited monoclinic ZrO_2 among these catalysts, so there were more activity sites that can adsorb and activate CO_2 on its surface than other catalysts. This result was confirmed by XPS and CO_2-TPD characterization (Figs. 4 and 6). As expected, the Ni_5-Cr_{10}/Zr nano-composite catalyst showed the highest CO_2 conversions in the catalytic performance experiment. No diffraction peaks of Cr_2O_3 and modifiers were observed on the XRD spectra of modified and unmodified Cr_2O_3/ZrO_2 nano-composites, probably due to their lower intensities or highly dispersed in the composites.

The TEM images of the modified Cr_2O_3/ZrO_2 nano-composites (Fig. 2) show that the Fe_5-Cr_{10}/Zr, Mn_5-Cr_{10}/Zr, Ni_5-Cr_{10}/Zr and Co_5-Cr_{10}/Zr nano-composites were regularly spherical in shape, and the size distribution of these nano-particles was very narrow. Nevertheless, the relatively good agreement between BET surface area and the particle size from TEM images indicated that single crystalline particles of all these samples were separable. Few solid agglomerates were observed for the Co_5-Cr_{10}/Zr nano-composite (Fig. 2d), which explains why its surface area was the smallest among these nano-composites (Table 2).

3.3. Characterization results of XPS

Surface Cr Species on modified and unmodified Cr_2O_3/ZrO_2 nano-composite catalysts were examined by XPS. The XPS

Table 2
Physical–chemical properties of various Cr_2O_3/ZrO_2 nano-composites

Catalysts	S_{BET} (m^2/g)	Pore volume (cm^3/g)	Average pore size (nm)	Particle size (nm)	Cr^{3+}BE (eV)	Cr^{6+}BE (eV)	Cr^{6+}/Cr^{3+}
Cr_2O_3/ZrO_2	147	0.23	4.88	7–12	576.3	578.8	1.11
Fe_5-Cr_{10}/Zr	172	0.51	11.79	5–7	576.2	578.9	2.70
Ni_5-Cr_{10}/Zr	163	0.53	12.90	5–9	576.2	578.9	1.91
Mn_5-Cr_{10}/Zr	144	0.42	11.63	5–8	576.3	579.0	1.78
Co_5-Cr_{10}/Zr	125	0.43	13.89	8–12	576.2	578.8	1.38

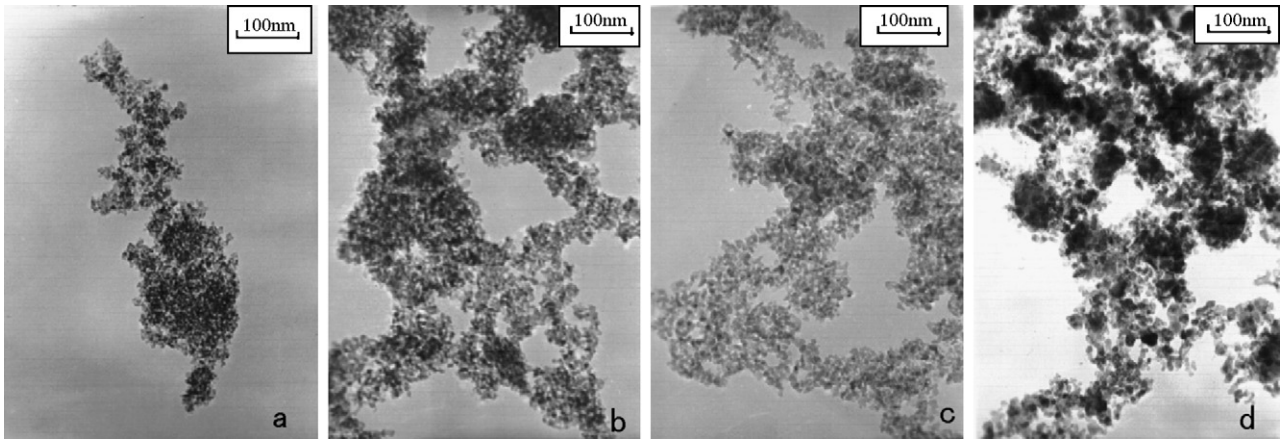

Fig. 2. TEM images of the modified Cr_2O_3/ZrO_2 nano-composites: (a) Fe_5-Cr_{10}/Zr; (b) Ni_5-Cr_{10}/Zr; (c) Mn_5-Cr_{10}/Zr; (d) Co_5-Cr_{10}/Zr.

spectra of Cr 2p on all catalysts are shown in Fig. 3. Two peaks occurred for Cr $2p_{3/2}$ spectra on all catalysts: one at ~576 eV and the other at ~579 eV. Those two species can be assigned to Cr^{3+} and Cr^{6+}, respectively [7]. The binding energy (BE) values of Cr $2p_{3/2}$ peaks were obtained by applying a peak-fitting program and given in Table 2. The binding energies (BE) for Cr^{3+} and Cr^{6+} on all catalysts were very similar, respectively. The addition of modifiers increased the Cr^{6+}/Cr^{3+} ratios of modified Cr_2O_3/ZrO_2 nano-composite catalysts, and the Fe_5-Cr_{10}/Zr nano-composite catalyst showed the greatest Cr^{6+}/Cr^{3+} ratio.

Some researches indicate that the active species for dehydrogenation on Cr_2O_3-based catalysts are Cr^{3+} or/and Cr^{2+} ions [18,19]. In recent years, Wang et al. [7] investigated the dehydrogenation of ethane with CO_2 over supported chromium oxide catalysts and proposed that surface Cr^{3+} species and Cr^{6+}/Cr^{3+} couples are the active sites for dehydrogenation of ethane. Ge et al. [20] used ESR and UV-DRS to probe the active site for the dehydrogenation of ethane with CO_2 over silica-supported chromium oxide catalysts, and found that species with high valet states (Cr^{5+} or Cr^{6+}) are important for the reaction. In this investigation, it was found that two Cr species, Cr^{3+} and Cr^{6+}, coexisted on the surface of modified Cr_2O_3/ZrO_2 nano-composite catalysts, and the Cr^{6+}/Cr^{3+} ratios on the catalysts were different. The ratio of Cr^{6+}/Cr^{3+} affects the acidity and/or reducibility of catalyst [21,22]. Therefore, these modified Cr_2O_3/ZrO_2 nano-composite catalysts exhibited very different catalytic activity.

Fig. 4 shows the XPS spectra of O 1s on modified and unmodified Cr_2O_3/ZrO_2 nano-composite catalysts. The Cr_2O_3/ZrO_2 nano-composite catalyst displayed one wide and unsymmetrical peak, suggesting the presence of two kinds of oxygen species with different chemical environments on its surface. The peak at lower binding energy (near 529.5 eV) can be assigned to surface lattice oxygen O^{2-} (hereafter denoted as O_I). The other peak at higher binding energy (near 531.0 eV) has been attributed to carbonates or adsorbed CO_2 (hereafter denoted as O_{II}) [23–25]. From the XPS spectra of C 1s over the Cr_2O_3/ZrO_2 nano-composite catalyst, a C 1s peak at 288.2 eV can be observed in addition to the C 1s peak of hydrocarbon contaminant carbon at 284.6 eV. Since the C 1s peak at 288.2 eV is due to carbonate species [26,27], the O 1s peak near 531.0 eV demonstrates the formation of some activity sites that can adsorb and activate CO_2 on the Cr_2O_3/ZrO_2 nano-composite catalyst surface.

The O 1s peaks of modified Cr_2O_3/ZrO_2 nano-composite catalysts were wider than the corresponding peak of the Cr_2O_3/

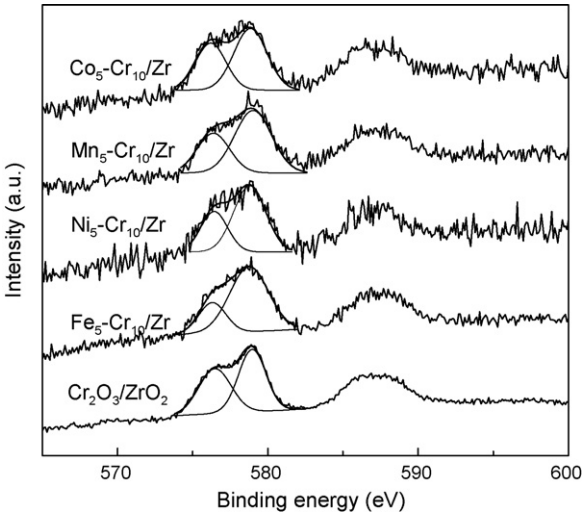

Fig. 3. XPS spectra of Cr 2p on various Cr_2O_3/ZrO_2 nano-composite catalysts.

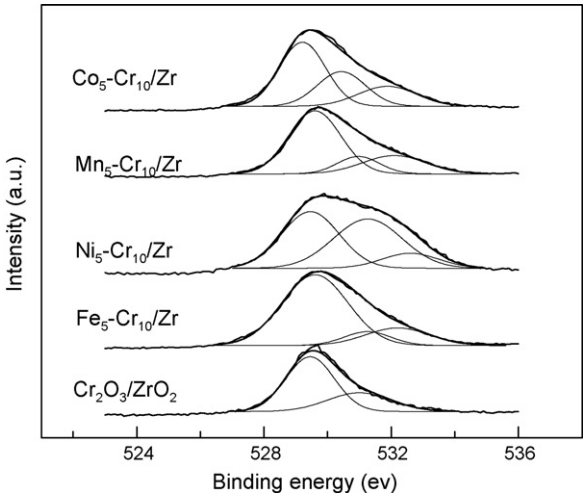

Fig. 4. XPS spectra of O 1s on various Cr_2O_3/ZrO_2 nano-composite catalysts.

Table 3
Analysis of O 1s on various Cr_2O_3/ZrO_2 nano-composite catalysts

Catalysts	O_I		O_{II}		O_{III}	
	Binding energy (eV)	Percent	Binding energy (eV)	Percent	Binding energy (eV)	Percent
Cr_2O_3/ZrO_2	529.50	67.37	531.05	32.63	–	–
Fe_5-Cr_{10}/Zr	529.57	70.38	531.00	10.56	532.20	19.06
Ni_5-Cr_{10}/Zr	529.41	41.30	531.21	46.21	532.78	12.49
Mn_5-Cr_{10}/Zr	529.58	56.97	530.88	18.51	532.15	24.52
Co_5-Cr_{10}/Zr	529.27	50.28	530.46	27.51	532.00	22.21

ZrO_2 nano-composite catalyst, and shoulder peaks were visible on their spectra (Fig. 4). These imply the formation of a new type of surface oxygen species. The binding energy (BE) values of O 1s peaks obtained by a fitting program are listed in Table 3. The new type of surface oxygen species (near 532 eV) has been reported to be adsorbed oxygen species (O^-, O_2^{2-}) (hereafter denoted as O_{III}) [24,28]. When Fe cations are doped into the crystal Cr_2O_3/ZrO_2 nano-composite replacing some Zr^{4+}, Cr^{3+} or Cr^{6+} cations, unbalanced charges and lattice distortion occur on the Fe_5-Cr_{10}/Zr nano-composite surface. Consequently, some oxygen vacancies probably present, which will be relinquished via adsorbing oxygen from environment [29,30]. Therefore, there were more adsorbed oxygen species (O_{III}) on the surface of the Fe_5-Cr_{10}/Zr nano-composite than the Cr_2O_3/ZrO_2 nano-composite catalyst. Absorbed oxygen species (O_{III}) also exited on the Ni_5-Cr_{10}/Zr, Mn_5-Cr_{10}/Zr, and Co_5-Cr_{10}/Zr nano-composites catalysts surface for the same reason.

The lattice oxygen species (O_I) are mainly responsible for selective oxidation of hydrocarbons, and adsorbed oxygen species (O_{III}) are involved in deep oxidation, leading to CO_x product formation [24,26]. However, other researches have shown that adsorbed oxygen species (O_{III}) may also participate in selective reaction steps on the catalytic surface of several metal oxides [27]. Our research indicated that proportions of lattice oxygen (O_I), oxygen species in adsorbed CO_2 (O_{II}) and adsorbed oxygen (O_{III}) on surfaces of all Cr_2O_3/ZrO_2 nano-composite catalysts were very different (Table 3). The Ni_5-Cr_{10}/Zr nano-composite catalyst exhibited the highest proportion of oxygen species in adsorbed CO_2 (O_{II}) among modified Cr_2O_3/ZrO_2 nano-composite catalysts, even more than the Cr_2O_3/ZrO_2 nano-composite catalyst, which means there were the most activity sites for CO_2 on its surface. Therefore, the Ni_5-Cr_{10}/Zr nano-composite catalyst exhibited the highest CO_2 conversion in the catalytic performance experiment. Comparing with the Cr_2O_3/ZrO_2 nano-composite catalyst, the proportion of adsorbed oxygen (O_{III}) on the Fe_5-Cr_{10}/Zr, Mn_5-Cr_{10}/Zr and Co_5-Cr_{10}/Zr nano-composite catalysts surface increased, and the proportion of oxygen species in adsorbed CO_2 (O_{II}) decreased. The catalytic performance experiment indicated that their ethylene selectivity increased remarkably, while their CO_2 and ethane conversion decreased, demonstrating that adsorbed oxygen species (O_{III}) are prone to reduce the reforming reaction. The Fe_5-Cr_{10}/Zr nano-composite catalyst exhibited not only the highest ethylene selectivity, but also high ethane and CO_2 conversion. These phenomena indicate that lattice oxygen (O_I), adsorbed oxygen species (O_{III}) and oxygen species in adsorbed CO_2 (O_{II}) play important roles in oxidative dehydrogenations of ethane with CO_2 to ethylene. The catalyst can exhibit good catalytic reaction activity if the proportion of these three kinds of oxygen species the on catalyst surface is proper.

3.4. Acid and base characteristics

It is generally believed that acid/base property is important factor in influencing catalytic activity. Acid–base pairs are important for hydrocarbon activation. CO_2 and NH_3 temperature programmed desorption were used to determine the base and acid properties of catalyst in this investigation, although there are several methods available for characterizing the acid and base

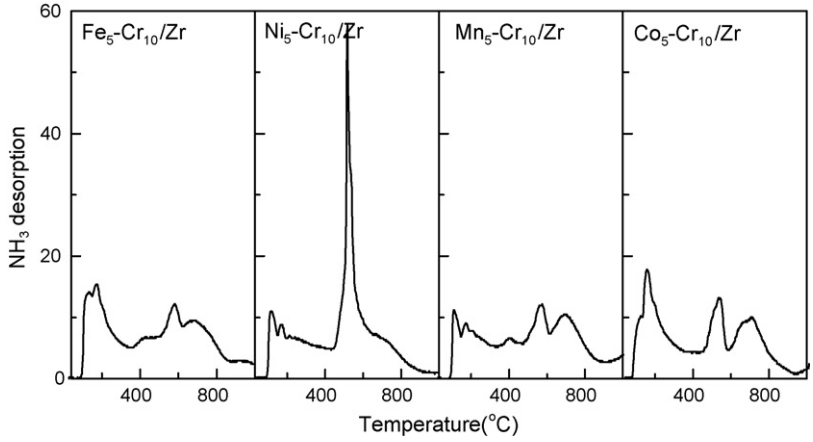

Fig. 5. NH_3-TPD profiles for various Cr_2O_3/ZrO_2 nano-composite catalysts.

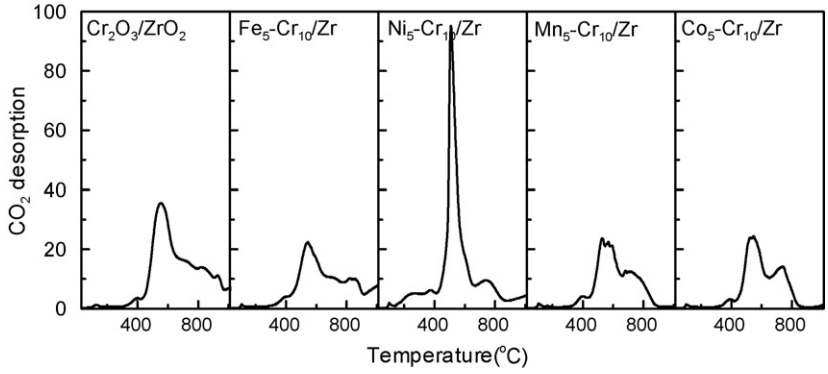

Fig. 6. CO_2-TPD profiles for various Cr_2O_3/ZrO_2 nano-composite catalysts.

properties of solids. The NH_3- and CO_2-TPD profiles for the Fe_5-Cr_{10}/Zr, Mn_5-Cr_{10}/Zr, Co_5-Cr_{10}/Zr, and Ni_5-Cr_{10}/Zr nano-composite catalysts are shown in Figs. 5 and 6, respectively. The results show that acidic and basic sites coexist on the surface of all catalysts. The modified Cr_2O_3/ZrO_2 nano-composite catalysts presented varying NH_3- and CO_2-TPD patterns, suggesting different numbers and strength of acid/base sites on their surfaces. Many peaks can be observed on the NH_3- and CO_2-TPD profiles of the modified Cr_2O_3/ZrO_2 nano-composite catalysts in the whole experimental region, from 50 to 1000 °C, which indicate the presence of many kinds of acid/base sites on their surfaces. The low-temperature desorption peak represents weak acid/base sites and the high-temperature desorption peak corresponds to strong acid/base sites on catalyst surface.

For the Ni_5-Cr_{10}/Zr nano-composite catalyst, a very large NH_3-desorption peak appeared from 450 to 600 °C (Fig. 5), indicating a large number of strong acid sites on its surface. The number of strong acid sites on the Fe_5-Cr_{10}/Zr, Mn_5-Cr_{10}/Zr and Co_5-Cr_{10}/Zr nano-composite catalysts were much smaller than that of the Ni_5-Cr_{10}/Zr nano-composite catalyst, because their desorption peaks at temperatures between 450 and 600 °C were much smaller than that of the Ni_5-Cr_{10}/Zr nano-composite catalyst. In the catalytic experiment, the ethylene selectivity of the Fe_5-Cr_{10}/Zr, Mn_5-Cr_{10}/Zr and Co_5-Cr_{10}/Zr nano-composite catalysts were markedly higher than that of the Ni_5-Cr_{10}/Zr nano-composite catalyst, which mainly favored the reforming and cracking reactions. It can be concluded that the strong acid sites promote the reforming and cracking reactions, and affect ethylene selectivity in the oxidative dehydrogenation of ethane with CO_2.

The Fe_5-Cr_{10}/Zr, Mn_5-Cr_{10}/Zr and Co_5-Cr_{10}/Zr nano-composite catalysts showed different area peaks at temperatures between 100 and 200 °C, meaning there were different numbers of weak acid sites on their surfaces, and these catalysts exhibited different reactant conversion. The order of ethane conversion of these catalysts was Co_5-Cr_{10}/Zr > Fe_5-Cr_{10}/Zr > Mn_5-Cr_{10}/Zr, which agreed with the order of the number of weak acid sites on their surfaces. So, it can be deduced that the weak acid sites are involved in ethane activation.

Fig. 6 indicates that the total area of CO_2 desorption peaks of the Ni_5-Cr_{10}/Zr nano-composite catalyst was the largest, which means there were more sites available for CO_2 absorption on its surface. This result was consistent with the XPS result. Except for the Ni_5-Cr_{10}/Zr nano-composite catalyst, there were no weak base sites on other Cr_2O_3/ZrO_2 nano-composite catalysts, induced by the absence of peaks on their CO_2-TPD profiles at temperatures between 100 and 250 °C.

Although all Cr_2O_3/ZrO_2 nano-composite catalysts presented varying CO_2-TPD patterns, a large peak occurred on every CO_2-TPD profiles between 450 and 650 °C. This implies the presence of strong base sites on their surfaces. The peak of the Ni_5-Cr_{10}/Zr nano-composite catalyst was the highest, which means the number of strong base sites was the greatest. After addition of Fe, Mn, and Co oxides, the peak of Cr_2O_3/ZrO_2 nano-composite catalysts at the temperatures between 450 and 650 °C decreased; however, the ethylene selectivity of the Fe_5-Cr_{10}/Zr, Mn_5-Cr_{10}/Zr and Co_5-Cr_{10}/Zr nano-composite catalysts increased in the catalytic activity experiment. So strong base sites decrease the ethylene selectivity, and strong acid–base pairs benefit the side reaction—the reforming and cracking reactions. These results clearly illustrate that the catalyst acid/base property also plays an important role in the oxidative dehydrogenation of ethane with CO_2. In combination with the XPS results, it can be concluded that the distribution of chromium species, oxygen species and base/acid property on the surface of catalyst cooperatively determined the catalytic activity of modified Cr_2O_3/ZrO_2 nano-composite catalysts in dehydrogenations of ethane to ethylene using CO_2 as an oxidant.

4. Conclusion

This investigation clearly shows that modified Cr_2O_3/ZrO_2 nano-composite catalysts exhibited varying activities in dehydrogenation of ethane with carbon dioxide. The modifiers of Fe, Co and Mn oxides markedly increased the ethylene selectivity of the Cr_2O_3/ZrO_2 nano-composite catalyst, while the Ni_5-Cr_{10}/Zr nano-composite catalyst mainly favored side reactions—the reforming and cracking reactions. Based on the ethylene yield, the catalytic activity of modified Cr_2O_3/ZrO_2 nano-composite catalysts at 650 °C followed the order of Fe_5-Cr_{10}/Zr > Mn_5-Cr_{10}/Zr > Co_5-Cr_{10}/Zr > Ni_5-Cr_{10}/Zr. The nature of the modifier exerted an influence upon the textural and structural property of catalyst, distribution of chromium species and oxygen species, and acid/base property of the catalyst surface, which in turn

determined the catalytic activity of the modified Cr_2O_3/ZrO_2 nano-composite catalysts in dehydrogenation of ethane with carbon dioxide.

Acknowledgements

This research was supported by the National Science Foundation of China (Grant no. 20436050), and National 863 Program Youth Foundation (Grant no.2004AA649230). The authors would like to thank Dr. Jessica Winter, assistant professor of Ohio State University, for checking and improving the English of this article.

References

[1] L. Xu, J. Liu, H. Yang, Y. Xu, Q. Wang, L. Lin, Catal. Lett. 62 (1999) 185–189.
[2] X. Zhang, A. Zhu, X. Li, W. Gong, Catal. Today 89 (2004) 97–102.
[3] J. Hong, D. Chang, V. Vladislav, Y. Jin, P. Sang-Eon, Stud. Surf. Sci. Catal. 153 (2004) 339–342.
[4] F. Solymosi, R. Nemeth, Catal. Lett. 62 (1999) 197–200.
[5] N. Mimura, I. Takahara, M. Inaba, M. Okamoto, K. Murata, Catal. Commun. 3 (2002) 257–262.
[6] O.V. Krylov, A.Kh. Mamedov, S.R. Mirzabekova, Catal. Today 24 (1995) 371–375.
[7] S. Wang, K. Murata, T. Hayakawa, K. Suzuki, Appl. Catal. A 196 (2000) 1–8.
[8] K. Nakagawa, C. Kajita, Y. Ide, M. Okamura, S. Kato, H. Kasuya, N. Ikenaga, T. Kobayashi, T. Suzuki, Catal. Lett. 64 (2000) 215–221.
[9] R.X. Valenzuela, G. Bueno, V.C. Corberan, Y. Xu, C. Chen, Catal. Today 61 (2000) 43–48.
[10] K. Nakagawa, M. Okamura, N. Ikenaga, T. Suzuki, T. Kobayashi, Chem. Commun. (1998) 1025–1026.
[11] X. Zhao, X. Wang, Catal. Commun. 7 (2006) 633–638.
[12] L. Liu, H. Li, Yi Zhang, Catal. Today 115 (2006) 235–242.
[13] W. Kuang, Y. Fan, C. Liu, K. Chen, Y. Chen, J. Chem. Res. 9 (1998) 610–611.
[14] H. Wang, J. Wang, W. Xiao, W. Yuan, Powder Technol. 111 (2000) 175–178.
[15] S. Deng, H. Li, Y. Zhang, Chinese J. Catal. 24 (2003) 744–750.
[16] B. Bachiller-Baeza, I. Rodriguez-Ramos, A. Guerrero-Ruiz, Langmuir 14 (1998) 3360–3556.
[17] K. Jung, A.T. Bell, J. Mol. Catal. A: Chem. 163 (2000) 27–42.
[18] H.J. Lugo, J.H. Lunsford, J. Catal. 91 (1985) 155.
[19] F.M. Ashmawy, J. Chem. Soc., Faraday Trans. 76 (1980) 2096.
[20] X. Ge, M. Zhu, J. Shen, React. Kinet. Catal. Lett. 77 (2002) 102–108.
[21] J. Sohn, S. Ryu, Catal. Lett. 74 (2001) 105–110.
[22] G. Neri, A. Pistone, S. De Rossi, E. Rombi, C. Milone, S. Galvagno, Appl. Catal. A 260 (2004) 75–86.
[23] S.G. Neophytides, S. Zafeiratos, S. Kennou, Solid State Ionics 136–137 (2000) 801–806.
[24] K. Tabata, Y. Hirano, E. Suzuki, Appl. Catal. A 170 (1998) 245–254.
[25] S. Ardizzone, C.L. Bianchi, B. Vercelli, Appl. Surf. Sci. 123 (1998) 169–175.
[26] M. Chen, X. Zheng, J. Mol. Catal. A 201 (2003) 161–166.
[27] L.M. Ioffe, P. Bosch, T. Viveros, H. Sanchez, Y.G. Borodko, Mater. Chem. Phys. 51 (1997) 269–275.
[28] H. He, H.X. Dai, Appl. Catal. A 251 (2003) 61–74.
[29] X. Wang, Y.-C. Xie, Appl. Catal. B 35 (2001) 85–94.
[30] N. Gunasekaram, N. Bakshi, C.B. Alcock, J.J. Carberry, Solid State Ionics 83 (1996) 145–150.